Compact surface plasmon-enhanced fluorescence biochip

Koji Toma,[1] Milan Vala,[2] Pavel Adam,[2] Jiří Homola,[2] Wolfgang Knoll,[1,3] and Jakub Dostálek[1,*]

[1]*AIT - Austrian Institute of Technology GmbH, Muthgasse 11, 1190 Vienna, Austria*
[2]*Institute of Photonics and Electronics, Academy of Sciences CR, Chaberská 57, 18251 Prague, Czech Republic*
[3]*Nanyang Technological University, Centre for Biomimetic Sensor Science, 637553 Singapore*
[*]*jakub.dostalek@ait.ac.at*

Abstract: A new concept of compact biochip for surface plasmon-enhanced fluorescence assays is reported. It takes advantage of the amplification of fluorescence signal through the coupling of fluorophore labels with confined and strongly enhanced field intensity of surface plasmons. In order to efficiently excite and collect the emitted fluorescence light via surface plasmons on a metallic sensor surface, (reverse) Kretschmann configuration is combined with diffractive optical elements embedded on the chip surface. These include a concentric relief grating for the imaging of highly directional surface plasmon-coupled emission to a detector. Additional linear grating is used for the generating of surface plasmons at the excitation wavelength on the sensor surface in order to increase the fluorescence excitation rate. The reported approach offers the increased intensity of fluorescence signal, reduced background, and compatibility with nanoimprint lithography for cost-effective preparation of sensor chip. The presented approach was implemented for biosensing in a model immunoassay experiment in which the limit of detection of 11 pM was achieved.

©2013 Optical Society of America

References and links

1. G. W. Ford and W. H. Weber, "Electromagnetic interactions of molecules with metal surfaces," Phys. Rep. **113**(4), 195–287 (1984).
2. V. Giannini, A. I. Fernández-Domínguez, Y. Sonnefraud, T. Roschuk, R. Fernández-García, and S. A. Maier, "Controlling light localization and light-matter interactions with nanoplasmonics," Small **6**(22), 2498–2507 (2010).
3. J. A. Schuller, E. S. Barnard, W. S. Cai, Y. C. Jun, J. S. White, and M. L. Brongersma, "Plasmonics for extreme light concentration and manipulation," Nat. Mater. **9**(3), 193–204 (2010).
4. J. W. Attridge, P. B. Daniels, J. K. Deacon, G. A. Robinson, and G. P. Davidson, "Sensitivity enhancement of optical immunosensors by the use of a surface-plasmon resonance fluoroimmunoassay," Biosens. Bioelectron. **6**(3), 201–214 (1991).
5. J. Dostálek and W. Knoll, "Biosensors based on surface plasmon-enhanced fluorescence spectroscopy," Biointerphases **3**(3), FD12–FD22 (2008).
6. E. Fort and S. Grésillon, "Surface enhanced fluorescence," J. Phys. D Appl. Phys. **41**(1), 013001 (2008).
7. J. R. Lakowicz, K. Ray, M. Chowdhury, H. Szmacinski, Y. Fu, J. Zhang, and K. Nowaczyk, "Plasmon-controlled fluorescence: a new paradigm in fluorescence spectroscopy," Analyst (Lond.) **133**(10), 1308–1346 (2008).
8. T. Liebermann and W. Knoll, "Surface-plasmon field-enhanced fluorescence spectroscopy," Colloids Surf. A Physicochem. Eng. Asp. **171**(1-3), 115–130 (2000).
9. M. E. Stewart, C. R. Anderton, L. B. Thompson, J. Maria, S. K. Gray, J. A. Rogers, and R. G. Nuzzo, "Nanostructured plasmonic sensors," Chem. Rev. **108**(2), 494–521 (2008).

10. L. Touahir, E. Galopin, R. Boukherroub, A. C. Gouget-Laemmel, J. N. Chazalviel, F. Ozanam, and S. Szunerits, "Localized surface plasmon-enhanced fluorescence spectroscopy for highly-sensitive real-time detection of DNA hybridization," Biosens. Bioelectron. **25**(12), 2579–2585 (2010).

11. K. Tawa, Y. Yokota, K. Kintaka, J. Nishii, and T. Nakaoki, "An application of a plasmonic chip with enhanced fluorescence to a simple biosensor with extended dynamic range," Sens. Actuators B Chem. **157**(2), 703–709 (2011).

12. J. R. Lakowicz, "Radiative decay engineering 3. Surface plasmon-coupled directional emission," Anal. Biochem. **324**(2), 153–169 (2004).

13. J. R. Lakowicz, J. Malicka, I. Gryczynski, and Z. Gryczynski, "Directional surface plasmon-coupled emission: a new method for high sensitivity detection," Biochem. Biophys. Res. Commun. **307**(3), 435–439 (2003).

14. J. S. Yuk, M. Trnavsky, C. McDonagh, and B. D. MacCraith, "Surface plasmon-coupled emission (SPCE)-based immunoassay using a novel paraboloid array biochip," Biosens. Bioelectron. **25**(6), 1344–1349 (2010).

15. M. Toma, K. Toma, P. Adam, J. Homola, W. Knoll, and J. Dostálek, "Surface plasmon-coupled emission on plasmonic Bragg gratings," Opt. Express **20**(13), 14042–14053 (2012).

16. R. R. Chance, A. Prock, and R. Silbey, "Molecular fluorescence and energy transfer near interfaces," Adv. Chem. Phys. **37**, 1–65 (1978).

17. K. Toma, J. Dostalek, and W. Knoll, "Long range surface plasmon-coupled fluorescence emission for biosensor applications," Opt. Express **19**(12), 11090–11099 (2011).

18. J. Enderlein and T. Ruckstuhl, "The efficiency of surface-plasmon coupled emission for sensitive fluorescence detection," Opt. Express **13**(22), 8855–8865 (2005).

19. A. Kinkhabwala, Z. F. Yu, S. H. Fan, Y. Avlasevich, K. Mullen, and W. E. Moerner, "Large single-molecule fluorescence enhancements produced by a bowtie nanoantenna," Nat. Photonics **3**(11), 654–657 (2009).

1. Introduction

Research in nano-scale emitters interacting with metallic surfaces [1] paved the way towards plasmonics – a modern branch of nanophotonics that focuses on the manipulation of light at sub-wavelength dimensions through its coupling with tightly confined field of surface plasmons [2, 3]. Over the last decade, these efforts flourished into increasing number of applications in fluorescence-based detection of molecular and biological analytes. In particular, new analytical tools with enhanced sensitivity and shorter analysis time were pursued based on plasmon-enhanced fluorescence (PEF) [4–7]. This method is also referred to as metal-enhanced fluorescence (MEF) and it offers an attractive means for the amplification of signal in fluorescence assays through the coupling of fluorophore labels with surface plasmons (SPs). It takes advantage of the enhanced field intensity of SPs on continuous metallic films [5, 8] as well as on metallic nanoparticles [9, 10] supported by structures that can be designed to increase the fluorophore excitation rate, collect and re-emit fluorescence light to certain directions, and improve fluorophore quantum yield through SPs.

Up to now, two main approaches utilizing propagating SPs for the amplification of fluorescence signal in biosensor applications were developed. In surface plasmon-enhanced fluorescence spectroscopy (SPFS), the binding of fluorophore-labeled molecules to biomolecular recognition elements attached to a metallic sensor surface is probed by SPs at the wavelength matching the fluorophore absorption band. This method was implemented by using Kretschmann configuration of attenuated total reflection (ATR) method [8] and metallic diffraction gratings [11]. The enhanced field intensity of SP increases the excitation rate of captured fluorophore-labeled molecules, which is directly translated to stronger fluorescence signal in SPFS. In surface plasmon-coupled emission (SPCE) [12, 13], highly directional fluorescence light emitted via surface plasmons is detected. Reverse Kretschmann configuration of ATR method [13, 14] and metallic diffraction gratings were mostly used in order to extract and re-emit the fluorescence light from a metallic sensor surface towards a detector. SPCE provides efficient means for collecting of fluorescence light and suppressing background signals. In this paper, we report a new approach to PEF biosensors with propagating SPs that makes it possible to simultaneously harness the advantages of both SPFS and SPCE. It is based on Kretschmann configuration combined with diffractive optical elements for the excitation of surface plasmons at the fluorophore absorption wavelength and for the imaging of surface plasmon-coupled emission at the emission wavelength to a detector. Design of these diffractive optical elements is discussed and the key performance

characteristics of the developed biochip are determined. The implementation to a compact PEF biochip is shown by using a model immunoassay experiment.

2. Materials and methods

2.1 Materials

Polydimethylsiloxane (PDMS) prepolymer SYLGARD® 184 and its curing agent were purchased from Dow Corning (USA). Amonil MMS10 was purchased from AMO GmbH (Germany). Photoresist S1818 was from Shipley (USA) and a developer AZ303 from Microchemicals (Germany) was used for its etching. Poly(methyl methacrylate) (PMMA) was from Sigma-Aldrich Handels (Austria). 1,1'-dioctadecyl-3,3,3′,3′-tetramethylindodicarbocyanine, 4-chlorobenzenesulfonate salt (DiD) was from Invitrogen (USA). This dye exhibits the absorption and emission bands centered at wavelengths of λ_{ab} = 644 nm and λ_{em} = 665 nm, respectively. Dithiolalkanearomatic PEG 6-COOH (COOH-thiol) and dithiolalkanearomatic PEG3-OH (PEG-thiol) were from SensoPath Technologies (USA). Phosphate buffered saline (PBS) with pH 7.4 was obtained from Calbiochem (Germany). PBS-Tween (PBS-T) buffer was prepared by adding 0.05% of Tween20 from Sigma-Aldrich (USA) to PBS buffer solution. Mouse immunoglobulin G (mIgG) and the antibody against this molecule (a-mIgG) were from Molecular Probes (USA). The a-mIgG was labeled by Alexa Fluor 647 with the dye-to-protein molar ratio of 4.5. This dye exhibits the absorption and emission wavelengths of λ_{ab} = 650 nm and λ_{em} = 668 nm, respectively. Rabbit immunoglobulin G (rIgG) was from Abcam (USA). 10 mM acetate buffer (ACT) with pH 5.5 was prepared from sodium acetate and acetic acid and the pH was adjusted by HCl and NaOH. 1-Ethyl-3-(3-dimethylaminopropyl) carbodiimide (EDC) and N-hydroxysuccinimide (NHS) were from Pierce (USA) and ethanolamine was from Sigma-Aldrich (USA).

2.2 Preparation of diffractive elements

Interference lithography (holography) was used for the preparation of master diffraction gratings. A positive photoresist layer (S1818, Shipley, USA) was spincoated on polished SF2 glass substrate and exposed to an interference field of two overlapping coherent beams from a HeCd laser (IK3031R-C from Kimmon Koha, Japan). Recorded gratings were etched by a developer AZ303 (diluted 1:9 with water), rinsed with water, and dried. Two types of relief grating structures were prepared – linear grating (LG) and concentric grating (CG). The LG element was prepared by an exposure of the photoresist layer to an interference field formed by two collimated laser beams. For the preparation of CG structure with a chirped periodic corrugation, an interference pattern of a collimated beam superimposed with a divergent beam was used [see Fig. 1(a)]. The chirped corrugation was recorded through a wedge-shaped mask that was sequentially rotated with an angular step δ in order to form a circular concentric structure. UV nanoimprint lithography (UV-NIL) was used for the transfer of master structures to the sensor chip based on the protocol described previously by our group [15]. As seen in Fig. 1(b), a master grating was casted to PDMS which was cured overnight at 60 °C. Afterwards, the PDMS was detached from the master and used further as a stamp. The PDMS stamp was placed onto about 150 nm thick layer of UV-curable polymer (Amonil) that was spin-coated on a glass substrate. The Amonil film in contact with the PDMS stamp was cured by UV light (irradiation dose of 36 J/cm^2 at a wavelength of λ = 365 nm) emitted from a UV lamp (Bio-Link 365, Vilber Lourmat, Germany), followed by the release of the PDMS stamp leaving a finished relief replica grating on the substrate. After the imprinting, the structured side of the substrate was coated with a gold layer by using sputtering (UNIVEX 450C, Leybold Systems, Germany). The thickness of the gold layer was of 50 nm on the flat sensing area in the middle of the CG element. The thickness of the gold layer on the CG and LG elements outside the sensing area was of 200 nm.
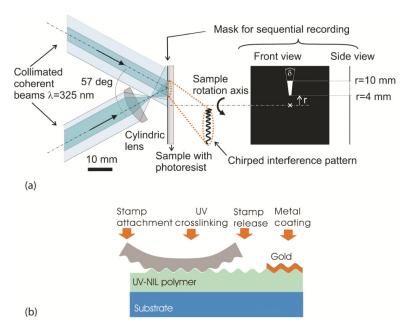
Fig. 1. (a) Preparation of the concentric grating element (CG) by using sequential recording into a photoresist by using interference lithography. (b) The transfer of grating elements onto the biochip surface by using UV-NIL.

2.3 Surface modification

For the testing of developed biochip, a 20 nm thick PMMA layer doped with DiD dye was used. This layer was deposited by using spin coating from a toluene solution with dispersed DiD dye at the concentration 700 nM and dissolved PMMA (1.4 wt.%). For the fluorescence immunoassay measurements, the 50 nm thick gold surface on the sensing area was modified with mIgG probe molecules. Firstly, the gold surface was immersed in a mixture of PEG-thiol and COOH-thiol dissolved in ethanol (molar ratio of 9:1 and total concentration of 1 mM) at the room temperature. After overnight incubation, the mixed thiol self-assembled monolayer (SAM) was formed and the surface was rinsed with ethanol and dried in a stream of nitrogen. Then, carboxylic terminal groups of COOH-thiol were activated by EDC and NHS solution (concentrations in deionized water of 75 and 21 mg/mL, respectively; 15 min incubation) and reacted for 90 min with mIgG molecules dissolved in ACT buffer at the concentration of 50 μg/mL. Finally, the unreacted active ester groups of the COOH-thiol were passivated by 20 min incubation in ethanolamine dissolved in water at 1 M concentration (pH of the solution adjusted to 8.5 by sodium hydroxide). In a control experiment, reference rIgG was immobilized on the biochip surface by using the same procedure.

2.4 Optical setups

For the observation of the spatial distribution of out-coupled SPCE, the fluorescence light beam that was emitted from the biochip was made incident at a diffuser which was placed at a distance D below its bottom surface, see Fig. 2(a). The scattered fluorescence light was imaged to an electron multiplying charge-coupled device (EM-CCD iXon + 885, Andor Technology, Ireland) by a camera lens (UNIFOC 58, Schneider Kreuznach, Germany). A set of filters including notch filter (XNF-632.8-25.0M, CVI Melles Griot, Germany) and band-pass filter (670FS10-25, LOT-Oriel, Germany) was used in order to suppres the background signal. For the investigation of the amplification of the fluorescence intensity by using the surface plasmon-enhanced excitation, the excitation light beam was coupled to the biochip by using the LG element and excited surface plasmons on the sensing area (2). As a reference,

fluorescence was excited directly with a light beam hitting the sensing area from above the biochip through water (1). In a model bioassay experiment, the SPCE signal outcoupled by the CG element was collected by a microscope objective (NA = 0.85, NT38-340, Edmund Optics, Germany) and its intensity F was measured in time by a photomultiplier tube (H6240-01, Hamamatsu, Japan) which was connected to a counter (53131A, Agilent, USA), see Fig. 2(b). For the excitation of the fluorescence, HeNe laser beam at the wavelength of λ_{ex} = 633 nm was used. This wavelength is sufficiently close to the absorption wavelengths λ_{ab} of DiD and AlexaFluor 647 dyes, taking into account the width of their absorption band of several tens of nanometers. In the model assay experiment, aqueous samples were pumped along the sensing area of the biochip by using a flow cell with the volume of around 10 μL that was casted to a PDMS.
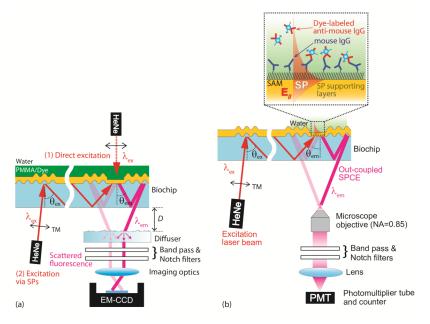

Fig. 2. Optical setups (a) for the observation of imaging properties of CG element and coupling efficiency of LG element and (b) for the model immunoassay experiment with the developed biochip.

2.5 Simulations

Finite element method (FEM) implemented in a grating solver DiPoG from Weierstrass Institute (Germany) was used for the calculation of the diffraction efficiency of relief metallic gratings. The chirped grating and the overall sensor chip geometry was designed by using a ray-tracing tool from Radiant Zemax (USA). For the simulation of surface plasmon-coupled emission, fluorophores were represented as randomly oriented dipoles and home-developed scripts based on the Chance-Prock-Silbey (CPS) model [16] were used as described in our previous works [17]. Refractive index of gold layer was of n_m = 0.118 + 3.92i at λ_{em} = 670 nm and n_m = 0.153 + 3.52i at λ_{ex} = 633 nm. Refractive indices of glass substrate and water of n_p = 1.51 and n_s = 1.33, respectively, were used for both λ_{ex} and λ_{em}.

3. Results and discussion

3.1 Surface plasmon-mediated fluorescence excitation and emission

The coupling of a fluorophore emission with surface plasmons strongly depends on the distance from a metal surface d. As simulations presented in Fig. 3 show, the maximum intensity of light emitted at λ_{em} = 670 nm is coupled to SPs on the gold surface in contact with

an aqueous medium at the distance around $d = 20$ nm. Below this distance, the emission is strongly quenched by Förster resonance energy transfer, while at larger distances $d>50$ nm the majority of light intensity is emitted to waves propagating into free space.
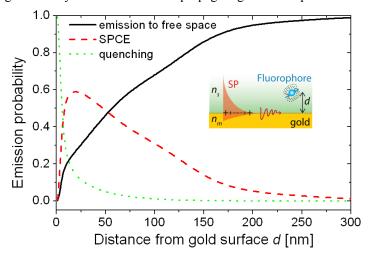

Fig. 3. Simulated emission probability from a randomly oriented dipole occurring via optical waves propagating into free space, surface plasmons (SPCE) and surface lossy waves (quenching) as a function of the distance from a metal surface d.

Assuming a thin gold film on a dielectric substrate, the fluorescence light emitted via SPs on its top can be out-coupled by reverse Kretschmann configuration of ATR and forms a characteristic SPCE cone propagating into the substrate, see Fig. 4. For randomly oriented fluorophores, this cone is directional in polar angle θ_{em} and isotropic in azimuthal angle ϕ. The dependence of the fluorescence intensity F on the polar angle θ_{em} was calculated for a fluorophore attached on the top of 20 nm thick spacer layer with a refractive index of $n_l = 1.5$, a gold film and a BK7 glass substrate. The results presented in Fig. 4 reveal that the SPCE intensity peaks at the polar angle $\theta_{em} = 72$ deg that is the surface plasmon resonance angle at $\lambda_{em} = 670$ nm. For the identical layer structure, electric field intensity enhancement $|\mathbf{E}/\mathbf{E_0}|^2$ at $d = 20$ nm was calculated as a function of the angle of incidence θ_{ex} at the excitation wavelength $\lambda_{ex} = 633$ nm. The obtained results show that strong field intensity builds up at the angle $\theta_{ex} = 74$ deg where the resonant coupling to SPs at λ_{ex} occur for the Kretschmann configuration of ATR. The thickness of the gold film of 50 nm was chosen for the excitation and out-coupling of surface plasmons by using the Kretschmann geometry. This thickness provides highest coupling strength of surface plasmons to an optical wave in the substrate and provides good directionality in SPCE (more detail studies can be found in literature [18]).
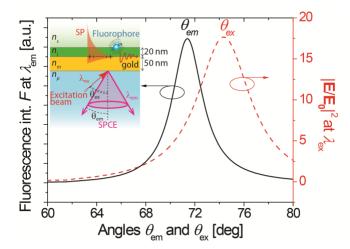
Fig. 4. Simulated dependence of the fluorescence intensity F of SPCE from a randomly oriented dipole at the distance $d = 20$ nm from the gold surface at the wavelength of $\lambda_{em} = 670$ nm (black solid line) on the polar angle θ_{em}. The electric field intensity enhancement $|E/E_0|^2$ at $d = 20$ nm due the excitation of SPs at the wavelength $\lambda_{ex} = 633$ nm is shown as a function of the angle of incidence θ_{ex} (red dashed line).

Let us note that the competing of non-radiative decay processes with the emission via surface plasmons allows for improving the quantum yield η of emitting dyes. This effect is particularly important for dyes with low quantum yield η for which highest enhancements of fluorescence signal were reported [19]. However, for relatively high quantum yield dyes that are typically used in fluorescence assays (and used in this work as well – DiD and Alexa Fluor 647) this effect is weak and leads rather to a decrease in total emitted light intensity due to the absorption in the metal [18].

3.2 Concept and design of PEF biochip based on diffractive optical elements

In order to exploit the fluorescence enhancement strategy based on the simultaneous excitation of fluorophore labels (at λ_{ex}) and the collecting of fluorescence light (at λ_{em}) via SPs, the biochip depicted in Fig. 5(a) was developed. It is composed of 1 mm thick BK7 glass substrate with a sensing area coated by a 50 nm gold film that carries biomolecular recognition elements for the specific capture of fluorophore-labeled target molecules. In order to collect the fluorescence light intensity emitted in the form of a SPCE cone at λ_{em}, a concentric relief grating (CG) element surrounding the sensing area was used. The grating is chirped in the radial direction in order to function as a diffraction lens that images the SPCE cone to a narrow spot below the biochip. The SPCE cone propagating in the glass substrate is totally internally reflected at the bottom surface of the substrate. Then it hits CG element that is coated with optically thick 200 nm thick gold film and is diffracted to a converging wave. The intensity of this wave focuses at a desired distance D below the biochip where a detector is placed, see Fig. 5(b). In order to couple the excitation beam at the wavelength λ_{ex} to SPs on the sensing area, a linear sinusoidal relief grating (LG) was employed. LG coated with 200 nm thick gold film allows the coupling of normal incident monochromatic beam at λ_{ex} to a wave that propagates in the glass substrate towards the sensing area by multiple total internal reflections at the bottom and top interfaces with the angle θ_{ex}. When hitting the sensing area coated with 50 nm thick gold film and aqueous sample on the top, the light beam excites SPs on the surface as this angle θ_{ex} coincides with SP resonance angle (see Fig. 4).
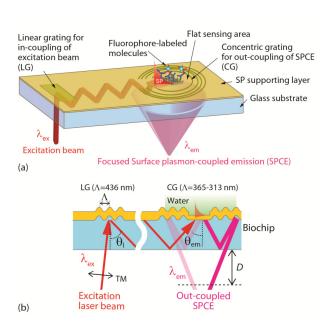
Fig. 5. (a) Schematic of the biochip with diffractive optical elements for the in-coupling of the excitation beam to the biochip (linear grating: LG) and for the out-coupling and imaging of surface plasmon-coupled emission (SPCE) to a detector (concentric grating: CG). (b) Side-view of the biochip.

The optimum period Λ and depth of CG and LG elements were determined based on a series of simulations. The CG element was designed to focus the SPCE beam with a wavelength of $\lambda_{em} = 670$ nm at a distance of around $D\sim15$ mm below the biochip surface. The dependence of the period Λ on the radial distance from the center r was chosen in order to diffract the SPCE beam incident at polar angles between $\theta_{em} = 67\text{-}77$ deg (see Fig. 4) via the -1st order. The optimum dependence $\Lambda(r)$ obtained from simulations is presented in Fig. 6 and it is compared with that of the prepared structure. These data shows an excellent agreement between targeted and prepared chirped grating. The periodic corrugation of CG element exhibited sinusoidal profile. In order to maximize the diffraction efficiency of this element, the (average) modulation depth of 120 nm was chosen based on the FEM simulations presented in Fig. 7(a). The AFM characterization showed a slightly lower (average) modulation depth of 110 nm of prepared CG structure.
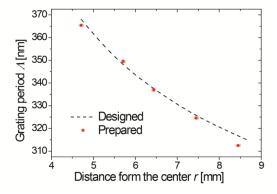

Fig. 6. Simulated (line) and measured (squares) dependence of the concentric grating (CG) period on the distance from its center.

The LG grating geometry was designed to couple a normal incident beam at $\lambda_{ex} = 633$ nm to a + 1st diffraction wave that propagates inside the glass substrate under an angle $\theta_{ex} = 74$ deg. This can be fulfilled for the period $\Lambda = 437$ nm. For the sinusoidal modulation depth the maximum diffraction efficiency of 34% occurs at the modulation depth 110 nm, see Fig. 7(b). The prepared characteristics of the prepared structures ($\Lambda = 436$ nm and depth 100 nm) matched the required parameters determined from simulations.
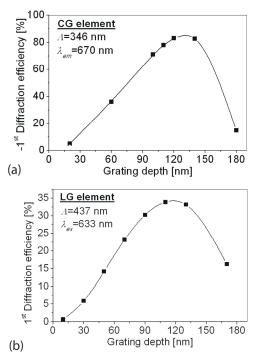

(a)

(b)

Fig. 7. Simulated diffraction efficiency in the ± 1st orders as a function of the grating depth for (a) the sinusoidal concentric grating (CG) element ($\Lambda = 346$ nm) for the TM polarized light beam incident at the emission angle $\theta_{em} = 71$ deg at the emission wavelength $\lambda_{em} = 670$ nm and (b) for the sinusoidal linear grating (LG) element with the period of $\Lambda = 437$ nm and normal incident TM polarized beam at the wavelength of $\lambda_{ex} = 633$ nm.

3.3 Imaging properties of concentric grating element

The imaging properties of CG were observed by measuring spatial distribution of out-coupled fluorescence light at the distance D from the biochip varied between 0 to 15 mm, see Fig. 8(a). The sensing area of the chip surrounded by CG was coated with 20 nm thick PMMA layer doped with DiD dyes (exhibiting similar characteristics to Alexa Fluor 647 used in further model immunoassay experiments). The top of the sensing area was brought in contact with water and exposed to a normal incident laser beam illuminating the area of ~1 mm². Let us note that in this experiment the majority of fluorescence light (emitted from DiD dyes dispersed at distances $d < 20$ nm from the surface) was quenched due to the Förster energy transfer. Even though, the emitted intensity was sufficiently strong to measure the outcoupling and imaging characteristics of the CG. As seen in Fig. 8(a), the intensity of out-coupled SPCE exhibits a characteristic ring distribution with a decreasing diameter when increasing the distance D (the bright spot in the middle of the ring originates from the fluorescence and scattered light transmitted perpendicular through the 50 nm thick gold film) The fluorescence beam focuses and reaches its minimum area at D~15 mm that is close to

that predicted by simulations. The diameter of the focused fluorescence spot depends on the angular step of CG segments δ [see Fig. 1(a)]. As Fig. 8(b) shows, the area of the spot decreases when decreasing δ and the width of the spot 0.7 mm (full width at half maximum - FWHM) was observed for the minimum angular step of $\delta = 3$ deg. Let us note that additional broadening of the focused fluorescence spot is caused by the finite size of the illumination area of the excitation beam and by the chromatic abberation of the CG lens.
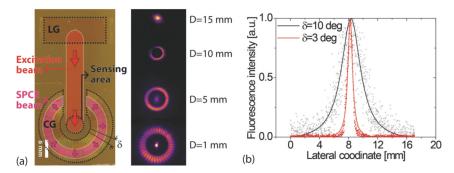

Fig. 8. (a) Top view of prepared biochip carrying LG and CG diffractive elements (left) and observed spatial distribution of out-coupled SPCE intensity at the distance below the biochip of $D = 1$, 5, 10 and 15 mm (right). (b) The cross-section of the fluorescence intensity at the distance of $D = 15$ mm for angular width of the CG element $\delta = 3$ and 10 deg.

The fluorescence intensity detected in the focal plane at the wavelength $\lambda_{em} = 670$ nm increases when dyes are excited with the enhanced field intensity of surface plasmons at the excitation wavelength $\lambda_{ex} = 633$ nm. In further experiments, the excitation laser beam was coupled to the biochip by using the LG element, propagated along the biochip substrate and excited SPs on the sensing area under the resonance angle $\theta_{ex} = 74$ deg. Only moderate enhancement ~1.9 ± 0.5 of the fluorescence light collected by SPCE was observed with respect to that measured for the normal incident beam from the top (data not shown). This is due to the relatively low diffraction efficiency of LG (reducing the intensity by a factor <0.34) and attenuation by multiple reflections at the surface between BK7 glass substrate and 200 nm thick gold (reducing the intensity by a factor <0.6) which decreases the excitation light intensity by a factor higher than ~5. Let us note that the using of an optimized LG grating with higher efficiency (e.g., blazed grating) and through removing the absorbing gold film from the path of the excitation beam can provide an increase in the fluorescence intensity by a factor of >10. This value is in agreement with the electric field intensity enhancement predicted by the simulations in Fig. 5.

3.4 Model immunoassay experiment

The kinetics of fluorescence signal upon the affinity binding of target molecules a-mIgG was measured by using the setup depicted in Fig. 2(b). In this experiment, a flow cell was attached to the sensing area on the biochip with immobilized mIgG probe molecules. Series of samples with concentration of a-mIgG between 30 pM to 1 nM were pumped through the flow cell with the flow rate of 0.503 mL/min. Each solution was flowed for 10 minutes followed by the 10 minutes rinsing with PBST. Figure 9(a) presents the measured fluorescence signal kinetics that is associated with the affinity binding of a-mIgG. It shows that the binding of the labeled a-mIgG to the surface modified with mIgG is manifested as a gradual increase of the fluorescence signal F in time. The slope of the fluorescence signal dF/dt linearly increases with the concentration of a-mIgG. In the control experiment, identical a-mIgG samples were flowed over the sensor surface that was modified with rIgG which is not specifically recognized by a-mIgG. The sensorgram in Fig. 9(a) shows negligible increase in the fluorescence signal, indicating the highly specific response. Using the kinetics data (measured

in triplicate), the calibration curve shown in Fig. 9(b) was obtained. For each a-mIgG concentration, the fluorescence signal slope dF/dt in the initial association phase was determined by linear fitting and plotted as a function of the concentration. The error bars represent the standard deviation (SD) that is attributed to the chip to chip variability. The limit of detection (LOD) of 11 pM was determined at the intersection where the sensor signal dF/dt matches 3-fold SD of the baseline fluorescence signal $3\sigma = 83$ cps min^{-1}. Let us note that the sensitivity of the presented assay is lower than that reported for regular SPCE and SPFS methods [5]. The reason is the that only a small fraction of SPCE signal was collected by the microscope objective (due to the large spot size of about 0.7 mm) and deliver to the detector, the excitation was weaker which is associated with the attenuating of the excitation beam, and possible background that originates from the auto-fluorescence from the excitation beam light propagating through the substrate was not blocked.
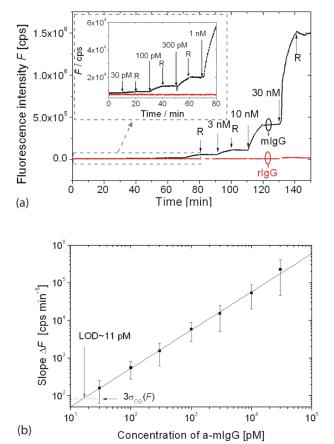

Fig. 9. (a) Measured binding kinetics $F(t)$ upon the sequential flow of samples with a-mIgG along the surface carrying the specific affinity partner mIgG (black) and control molecules rIgG (red). The inserted graph shows the magnified fluorescence intensity $F(t)$ for the concentration from 30 pM to 1 nM. b) Calibration curve of the developed biochip fitted with a linear function. The baseline noise and LOD are indicated.

4. Conclusions

A compact biochip for sensitive fluorescence-based assays was developed and its performance characteristics were discussed. The amplification of fluorescence signal by combining surface plasmon-enhanced excitation and surface plasmon-coupled emission was implemented by using two diffractive elements – linear and concentric gratings. The biochip

was prepared by UV-nanoimprint lithography from masters fabricated by interference lithography and is thus compatible with mass production technologies. The integration of the key optical elements to the biochip provides new means for combined SPFS and SPCE measurements which does not rely on bulky optical components (such as those with optical prism) and allows to overcome the fluorescence excitation through analyzed sample (as is needed for the amplification with diffraction grating-coupled SPR). Therefore, the reported biochip holds potential for substantial simplification of the sensor design, opening avenues for the development of compact portable devices for the use in the field. The preliminary data from a model immunoassay experiment show that the biochip provided sensitivity enabling the detection of IgG molecules at concentrations as small as 11 pM.

Acknowledgments